ACS APPLIED MATERIALS & INTERFACES

Letter

www.acsami.org

Thermally Activated Delayed Fluorescence Sensitized Phosphorescence: A Strategy To Break the Trade-Off between Efficiency and Efficiency Roll-Off

Chen Li, Lian Duan,* Dongdong Zhang, and Yong Qiu

Key Lab of Organic Optoelectronics & Molecular Engineering of Ministry of Education, Department of Chemistry, Tsinghua University, 100084 Beijing, China

Supporting Information

ABSTRACT: Materials with thermally activated delayed fluorescence (TADF) realized 100% internal quantum efficiency (IQE) but suffered significant efficiency roll-off. Here, an exciton dynamics study reveals that materials with TADF may play opposite roles in affecting the efficiency roll-off: decreasing the triplet density due to the fast reverse intersystem crossing, on the one hand, and increasing the triplet density due to the weakened singlet radiation. We show theoretically and experimentally that TADF-sensitized phosphorescence can break this trade-off by exploiting the efficient Förster energy transfer and simultaneously achieve 100% IQE and low efficiency roll-off (with a critical current density of 460 mA cm^{-2}).

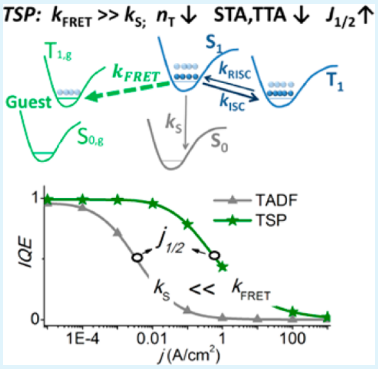

KEYWORDS: *exciton dynamics, quantum efficiency, efficiency roll-off, organic light-emitting diodes, exciton annihilation*

The progress of organic light-emitting diodes (OLEDs) has stimulated interest for their high-brightness applications in, for instance, organic lighting,[1] picoprojectors,[2] and electrically pumped organic lasers.[3] For high-brightness applications, devices that can realize high efficiency at high brightness are desired. However, the efficiency of OLEDs decreases significantly with increasing current density (j) or brightness (a well-known phenomenon called efficiency roll-off[4]). Efficiency roll-off can be quantified by the critical current density ($J_{1/2}$), the current density at which the quantum efficiency drops to half of its maximum value.[4] While ideal OLEDs for high-brightness applications require both high quantum efficiency and $J_{1/2}$, these two merits are hard to achieve simultaneously in traditional strategies for OLEDs.

For phosphorescent (PH) devices, although an internal quantum efficiency (IQE) close to unity has been achieved by taking advantage of the spin−orbit coupling in metal−organic complexes,[6,7] the efficiency roll-off is always very strong mostly owing to strong triplet−triplet annihilation (TTA) induced by the intrinsically high triplet density.[8,9] Fluorescent (FL) devices instead show higher critical current densities owing to the relatively low quenching rates of singlets.[10] However, their IQE values are typically lower than 25% because of the spin statistics limit under electrical driving conditions.[11]

A possible way to bring high IQE and $J_{1/2}$ together is to break the spin statistics limit of fluorescence. The efforts include TTA delayed fluorescence and thermally activated delayed fluorescence (TADF). In TTA delayed fluorescence, the triplets positively contribute to the fluorescence through TTA at low j, while decreasing the efficiency at higher j through singlet−triplet annihilation (STA).[12] As a result, $J_{1/2}$ comparable to that of the FL devices has been achieved. However, the upper limit of the triplet harvesting efficiency through the multiple TTA process is 37.5%[13] or 62.5%.[12] The recent breakthrough in TADF OLEDs has realized FL yields close to unity by converting the nonradiative triplets to radiative singlets through thermally activated reverse intersystem crossing (RISC).[14,15] Unfortunately, the efficiency roll-off is often found to be serious (Table S1 in the Supporting Information, SI). While the long lifetime of the delayed singlet lifetime is often to blame,[16] the mechanism of their efficiency roll-off remains elusive. Recently, we used 2-phenyl-4,6-bis(12-phenylindolo[2,3-*a*]carbazol-11-yl)-1,3,5-triazine (PBICT) as the host for tris(2-phenylpyridine)iridium [Ir(ppy)$_3$] to fabricate host−guest PH OLEDs.[17] High efficiency and low efficiency roll-off were noticed. However, the mechanism of their efficiency roll-off was not thoroughly discussed.

Here, an exciton dynamics study reveals that STA and TTA are the main origins for efficiency roll-off in TADF OLEDs. To suppress STA and TTA by lowering the triplet density, both small singlet−triplet splitting (ΔE_{ST}) and large singlet radiative rate (k_s) are indispensable. However, small ΔE_{ST} is intrinsically accompanied by small k_s. We demonstrate that the strategy of TADF-sensitized phosphorescence (TSP) can break this trade-

Received: May 12, 2015
Accepted: July 9, 2015
Published: July 9, 2015

DOI: 10.1021/acsami.5b04090
ACS Appl. Mater. Interfaces 2015, 7, 15154−15159

off by utilizing the more efficient Förster resonance energy transfer (FRET) rather than singlet radiation.

To investigate the effect of thermally activated RISC on the efficiency roll-off, exciton processes containing exciton generation, ISC, RISC, TTA, STA, singlet−singlet annihilation (SSA), and exciton polaron annihilation (SPA or TPA) are considered (Figure 1). To analyze the TSP process, FRET

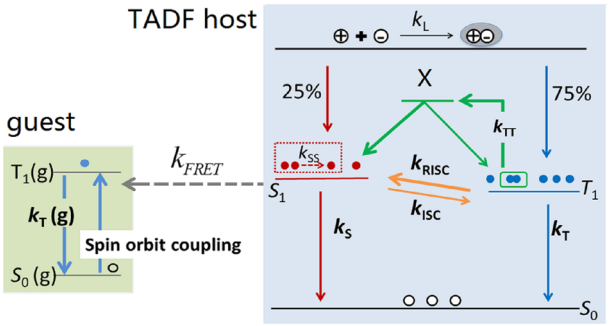

Figure 1. Exciton dynamics in a TADF host and an efficient PH guest. Red and blue full circles respectively represent the singlets and triplets. Open circles represent the ground states.

between the emission of the host and the PH guest is also introduced. The exciton generation process is described by[18]

$$\frac{dn_P}{dt} = \frac{j}{ew} - k_L {n_P}^2 \quad (1)$$

where n_P is the polaron density, j the current density, e the elementary charge, w the charge recombination layer thickness, and k_L the Langevin recombination rate constant.[19] We assume a balanced hole mobility (μ_h) and electron mobility (μ_e) with a charge recombination factor of 1. The TTA process follows one of two pathways:

$$T_1 + T_1 \xrightarrow{k_{TT}} X \begin{cases} \xrightarrow{1-\alpha} T_1 + S_0 \\ \xrightarrow{\alpha} S_1 + S_0 \end{cases} \quad (2)$$

where k_{TT} is the TTA rate constant. Here we assume α to be 25%.[4] Thus, this process would lead to a singlet generation rate constant of $^1/_8 k_{TT}$ and a triplet attenuation rate constant of $^5/_8 k_{TT}$. We note that α may be larger than 25% in some FL systems.[12] The SSA, STA, SPA, and TPA processes are described by[12,20,21]

$$S_1 + S_1 \xrightarrow{k_{SS}} S_1 + S_0 \quad (3)$$

$$S_1 + T_1 \xrightarrow{k_{ST}} S_0 + T_1 \quad (4)$$

$$S_1/T_1 + P \xrightarrow{k_{SP}/k_{TP}} S_0 + P^* \quad (5)$$

where k_{SS}, k_{ST}, k_{SP}, and k_{TP} are the SSA, STA, SPA, and TPA rate constants, respectively. Thus, the exciton dynamics can be described as

$$\frac{dn_S}{dt} = \frac{1}{4}k_L {n_P}^2 - \frac{1}{2}k_{SS}{n_S}^2 - (k_{ISC} + k_S + k_{ST}n_T + k_{SP}n_P) n_S + k_{RISC}n_T + \frac{1}{8}k_{TT}{n_T}^2 \quad (6)$$

$$\frac{dn_T}{dt} = \frac{3}{4}k_L {n_P}^2 - \frac{5}{8}k_{TT}{n_T}^2 - (k_{RISC} + k_T + k_{TP}n_P)n_T + k_{ISC}n_S \quad (7)$$

where n_S is the singlet density, n_T the triplet density, k_S the singlet radiative rate constant, k_T triplet radiative rate constant, k_{ISC} the ISC rate constant, and k_{RISC} and the RISC rate constant. When eqs 1, 6, and 7 are solved under steady state, the IQE of FL can be described as

$$IQE = k_S n_S/(j/ew) \quad (8)$$

The parameters used in the calculations (Table 1) refer to the typical values in the literature. k_L is calculated by $e(\mu_h + \mu_e)/(\varepsilon_r \varepsilon_0)$,[19] assuming $\mu_h = \mu_e = 1 \times 10^{-4}$ cm^2 V^{-1} s^{-1}. k_{RISC} is described as $k_{ISC}\exp(-\Delta E_{ST}/kT)$,[25] where k is the Boltzmann constant. For TADF or FL materials, k_{TT} is on the order of 10^{-15} cm^{-3} s^{-1},[24] while for PH materials, k_{TT} is controlled by Dexter transfer and has a larger value on the order of 10^{-12} cm^{-3} s^{-1}.[4]

Table 1. Parameters Used in the Calculations

parameter	value	ref
w/nm	20	
k_L/cm^{-3} s^{-1}	4.5×10^{-11}	
k_S/s^{-1}	0.9×10^{8} [a]	22
k_{ISC}/s^{-1}	1×10^{7} [a]	22
k_{ST}/cm^{-3} s^{-1}	1.9×10^{-10} [a]	21
k_{SP}/cm^{-3} s^{-1}	3×10^{-10} [a]	21
k_{SS}/cm^{-3} s^{-1}	6×10^{-11} [a]	22
k_T/s^{-1}	8×10^{5} [b]	23
k_{TP}/cm^{-3} s^{-1}	5.6×10^{-13} [b]	23
k_{TT}/cm^{-3} s^{-1}	3×10^{-12} [b]/ 5×10^{-15} [c]	23 and 24

[a]Values of tris(8-hydroxyquinoline)aluminum. [b]Values of Ir(ppy)$_3$. [c]Value of 4,5-bis(9*H*-carbazol-9-yl)phthalonitrile, a typical TADF material.

IQE and exciton density as a function of j for the FL, PH, TTA-FL, and TADF devices are calculated and depicted in Figure 2. The theoretical maximum IQE values for the FL, PH, and TTA devices are respectively 25%, 100%, and 40%, respectively. Both n_S and n_T increase almost linearly with j at low j but sublinearly with j at high j, showing the nature of roll-off. For the FL and TTA-FL devices, ISC merely leads to an efficiency reduction of a constant proportion and has a negligible effect on the efficiency roll-off. STA contributes to most of the efficiency roll-off at the operating j region. For the PH device, TTA is the main cause for efficiency loss at the operating j region. The TADF device with a ΔE_{ST} of 0.1 eV (Figure 2d) shows a maximum IQE of 98%, which is comparable to that of the PH device, and a $J_{1/2}$ value of 0.08 A cm^{-2}, which is much larger than that of the PH device. The increased fluorescent efficiency can be ascribed to the upconversion of triplets through RISC, and the increased $J_{1/2}$ can be ascribed to the sharply decreased STA at the operating j region. Besides, the roll-off of the triplet density induced by TTA is converted to the roll-off of the delayed fluorescence through RISC.

To quantify the contribution of each exciton dynamics process to the efficiency roll-off, we introduce the concept of fractional efficiency (FE), which is the ratio of the rate of one process to the fluorescent radiative rate. FE of STA is described as

DOI: 10.1021/acsami.5b04090
ACS Appl. Mater. Interfaces 2015, 7, 15154−15159

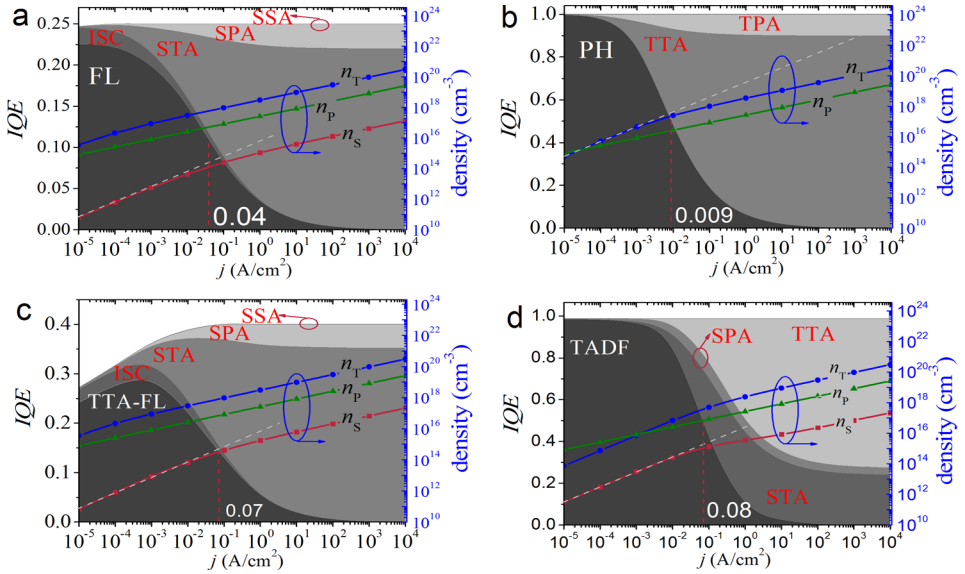

Figure 2. Simulated IQE (black edges), exciton density, and polaron density plotted with the current density (j) for the FL (a), PH (b) TTA-FL (c), and TADF (d) OLEDs. The contributions of the exciton dynamics processes on the efficiency loss are labeled in red font. The gray dashes refer the densities under no efficient roll-off, and the red dashes designate $J_{1/2}$. In the TADF situation (d), all processes are considered with a ΔE_{ST} value of 0.1 eV. In the FL situation (a), we assume no TTA fluorescent and RISC. In the PH situation (b), we assume no RISC and an ultraefficient ISC process so the singlet density is close to 0 under steady state. In the TTA-FL situation (c), no RISC is taken into account. k_T for the simulations in parts a, c, and d is set to 1×10^3 s^{-1}.

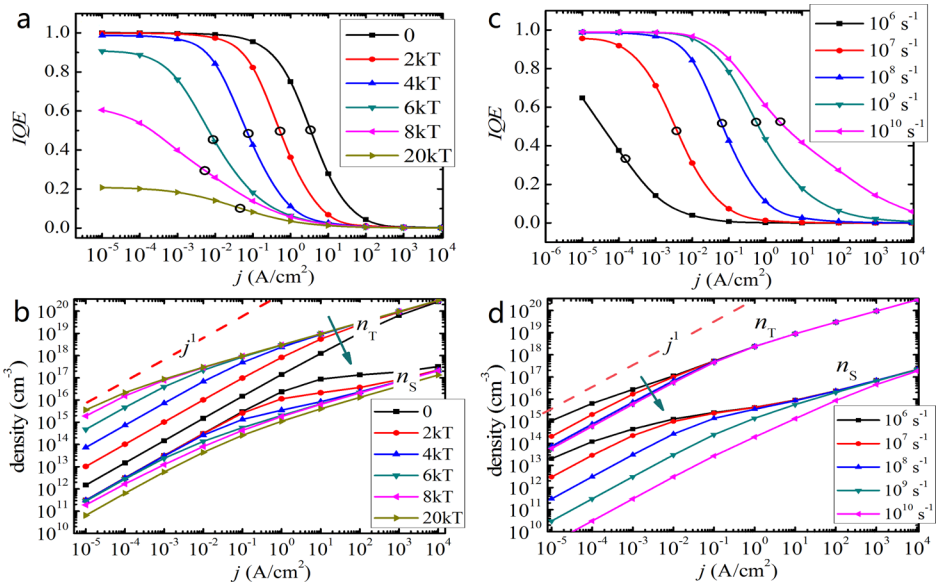

Figure 3. (a) IQE versus j at various ΔE_{ST} and (b) exciton densities versus j at various ΔE_{ST}. k_S used in parts a and b is 1×10^8 s^{-1}. $\Delta E_{ST} = 20kT$ refers to the traditional FL device. (c) IQE versus j at various k_S and (d) exciton densities versus j at various k_S. ΔE_{ST} used in parts c and d is 0.1 eV. Black circles designate $J_{1/2}$. Red dashes refer to the density $\propto j$.

$$\mathrm{FE_{STA}}(j) = k_{ST} n_S(j)\, n_T(j)/k_S n_S(j) = k_{ST} n_T(j)/k_S \quad (10)$$

Equation 10 suggests that the contribution of STA to the efficiency loss is proportional to$n_T(j)$. The increasing $n_T(j)$ with j is the origin of efficiency roll-off caused by STA. Similarly, $\mathrm{FE_{SPA}}$ and $\mathrm{FE_{SSA}}$ are respectively proportional to$n_P(j)$ and $n_S(j)$. However, SSA (or SPA) is always nonessential because of the much smaller n_S (or n_P) than n_T. For ISC and RISC, FE can be described as

$$\mathrm{FE_{ISC}}(j) = k_{ISC} n_S(j)/k_S n_S(j) = k_{ISC}/k_S \quad (11)$$

$$\mathrm{FE_{RISC}}(j) = k_{RISC} n_T(j)/k_S n_S(j) \quad (12)$$

Equation 11 indicates that the contribution of ISC to IQE loss is a constant; that is why ISC has no influence on the efficiency roll-off. Equation 12 suggests that the contribution of RISC to the efficiency roll-off of the TADF device is from n_T to n_S. The roll-off of n_T is mainly caused by TTA. From Figure 2d, we see that when $j > 0.1$ A cm^{-2}, TTA, instead of STA, becomes the main cause of the efficiency roll-off.

Consistent with the analysis by Murawski et al.,[4] it is found that STA is the dominant process for the fluorescent efficiency roll-off. When RISC is introduced, the influence of TTA also becomes significant. Both intensities of the two processes depend highly positively on the triplet density. Thus, the larger

DOI: 10.1021/acsami.5b04090
ACS Appl. Mater. Interfaces 2015, 7, 15154−15159

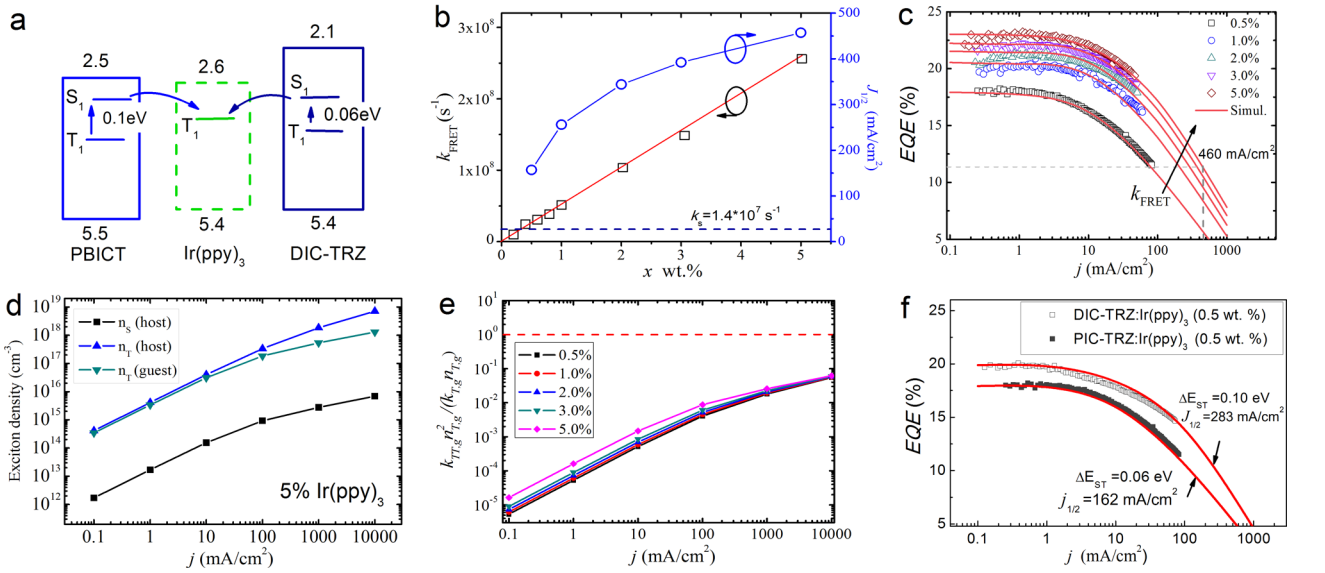

Figure 4. (a) Energy level diagram of the emitting layer. (b) Experimental k_{FRET} of PBICT/Ir(ppy)$_3$ films and the simulated $J_{1/2}$ of the OLEDs at various Ir(ppy)$_3$ concentrations. (c) Experimental and simulated EQE−j curves of the PBICT/Ir(ppy)$_3$ devices. (d) Exciton densities versus j for the PBICT/Ir(ppy)$_3$ (5 wt %) device. (e) Ratio between the TTA rate and triplet radiative rate versus j for PBICT/Ir(ppy)$_3$ devices with various x. (f) Experimental and simulated EQE−j curves of the PBICT/Ir(ppy)$_3$ (0.5 wt %) and DIC-TRZ/Ir(ppy)$_3$ (0.5 wt %) devices.

$J_{1/2}$ of the TADF device than those of the FL, PH, and TTA-FL devices (Figure 2) can be ascribed to its much smaller triplet density than those of the other three devices (Figure S2 in the SI). According to eq 12, the coefficients that directly affecting the contribution of RISC to TADF's efficiency roll-off are k_{RISC} and k_S, so their influences on the efficiency roll-off are studied in detail.

The influence of k_{RISC} is investigated by varying ΔE_{ST} in the simulation. Both IQE and $J_{1/2}$ increase as ΔE_{ST} decreases (Figure 3a). For the limiting case (ΔE_{ST} = 0kT), IQE of 1 and $J_{1/2}$ of 6 A cm^{-2} are achieved. At ΔE_{ST} larger than 6kT (0.15 eV at 298 K), $J_{1/2}$ values are smaller than that of the traditional FL device (for which we suppose a ΔE_{ST} of 20kT). Because the singlets of the TADF device are comprised of those from prompt fluorescence and RISC, the larger efficiency roll-off of TADF than that from prompt fluorescence at large ΔE_{ST} should originate from the roll-off of n_T. According to Figure 3b, when ΔE_{ST} > 4kT, the decrease of n_T through RISC is not significant, while n_S increases by orders through this process. As a result, the significant roll-off of n_T greatly increases the efficiency roll-off of the TADF device. However, as ΔE_{ST} decreases to small values, n_T decreases by orders of magnitude due to the efficient RISC, leading to decreased TTA and STA. The $J_{1/2}$ values of the reported TADF devices (Figure S1 in the SI) also show negative correlation with ΔE_{ST}.

IQE as a function of j at various k_S is depicted in Figure 3c. It shows clearly that increasing k_S can greatly decrease the efficiency roll-off. Ceteris paribus, as k_S increases from 1 × 10^6 to 1 × 10^{10} s^{-1}, $J_{1/2}$ increases from 0.2 to 4 A cm^{-2}. The decrease of the efficiency roll-off can also be ascribed to the decreased n_T, as shown in Figure 3d. For a constant ΔE_{ST}, increasing k_S will increase the radiative efficiency (ϕ_S) and decrease the ISC efficiency (ϕ_{ISC}), thus decreasing n_T in the multiple ISC−RISC circulations.

To take advantage of the small efficiency roll-off of the TADF device, both small ΔE_{ST} and large k_S are requested. Simulation at the limit situation (with ΔE_{ST} = 0.01 eV and k_S = 1 × 10^9 s^{-1}) even indicates $J_{1/2}$ of 40 A cm^{-2} (Figure S3 in the SI). However, a small ΔE_{ST} is attainable in molecules containing spatially separated donor and acceptor moieties, which would inevitably lead to low k_S according to Fermi's golden rule.[26] Thus, OLEDs using TADF emitters with small ΔE_{ST} always suffer serious efficiency roll-off owing to the emitters' small k_S.

Recently, OLEDs using TADF materials as sensitizing hosts have shown high external quantum efficiency (EQE).[27,28] These devices have the advantage of optimizing ΔE_{ST} of the host and k_S of the emitter separately. Here, we demonstrate theoretically that TSP can be feasible to achieve small efficiency roll-off by exploiting the much larger FRET rate constant (k_{FRET}) rather than k_S. According to the FRET theory, k_{FRET} can be described as[29]

$$k_{FRET} = k_S R_F^{\ 6}/r_{h-g}^{\ 6} \quad (13)$$

where R_F is the Förster radius of the host−guest pair, r_{h-g} is the distance between the donor and acceptor molecules. $R_F^{\ 6}$ is proportional to the overlap integral of the host's emission spectral and guest's absorption spectral. For materials with small ΔE_{ST}, while k_S is limited by Fermi's golden rule, k_{FRET} can be much larger than k_S by introducing guests with large R_F and efficient PH radiation. To confirm this conception, the efficiency roll-off of the PBICT/Ir(ppy)$_3$ (x wt %) OLEDs is discussed in detail (see the SI for the device structure).

The photophysical properties of PBICT have been investigated recently. PBICT has ΔE_{ST} of 0.1 eV (Figure 4a) and balanced hole/electron mobility around 1 × 10^{-4} cm^2 V^{-1} s^{-1}.[17] Its emission spectral well overlaps the triplet metal-to-ligand charge transfer absorption of Ir(ppy)$_3$,[17] enabling efficient singlet−triplet FRET. The FRET rates of PBICT/Ir(ppy)$_3$ films are derived by comparing the singlet lifetime (τ_s) to that of the pure PBICT film (Table S2 in the SI). Figure 4b shows that k_{FRET} increases with increasing concentration (x wt %) of Ir(ppy)$_3$ and is much larger than k_S of PBICT even at small x. The reason is that r_{h-g} decreases with increasing guest

DOI: 10.1021/acsami.5b04090
ACS Appl. Mater. Interfaces 2015, 7, 15154−15159

concentration and becomes smaller than R_F when $x > 0.2$ ($k_{FRET} > k_S$).

EQE simulations of the OLEDs are also carried out for a quantitative analysis. Upon the introduction of FRET, the dynamics of n_S in the host is adjusted to

$$\frac{dn_S}{dt} = \frac{1}{4}\frac{j}{ew} - \frac{k_{SS}n_S^2}{2} - \left(\frac{1}{\tau_S} + k_{ST}n_T + k_{SP}n_P\right)n_S + k_{RISC}n_T + \frac{k_{TT}n_T^2}{8} \quad (14)$$

where $1/\tau_S = k_{FRET} + k_S + k_{ISC}$. k_{SS}, k_{ST}, k_{SP}, and k_{TT} used are from Table 1. w is 30 nm according to the device structure. The triplet dynamics in the $Ir(ppy)_3$ emitter can be described as

$$\frac{dn_{T,g}}{dt} = k_{FRET}n_S - k_{T,g}n_{T,g} - \frac{5}{8}k_{TT,g}n_{T,g}^2 - k_{TP}n_{T,g}n_P \quad (15)$$

where the subscript g represents the parameters of the $Ir(ppy)_3$ guest, of which the rate constants are adapted from Table 1. The values of k_{FRET} and τ_s are from Table S2 in the SI. The nonradiative decay of $Ir(ppy)_3$ is neglected owing to its high PL efficiency of 0.97.[30] EQE through the emission of $Ir(ppy)_3$ is described as $\eta_{out}k_{T,g}n_{T,g}/(j/ew)$, where η_{out} is the out-coupling efficiency, which is set to 25%.

Simulations of the EQE−j curves of the PBICT/$Ir(ppy)_3$ OLEDs are shown in Figure 4c. The simulation results well fit with the experimental ones. As k_{FRET} increases (from 3×10^7 to 2.5×10^8 s^{-1}) with increasing x (from 0.5 to5), the maximum EQE increases from 17.5% to 23.1% and the efficiency roll-off becomes smaller. The experimental results indicate that increasing k_{FRET} has an effect on the device efficiency similar to that for increasing k_S. At $x > 5$, the roll-off is no longer improved (Figure S5 in the SI) because ϕ_{FRET} is saturated and n_T decreases very slowly when k_S is large (Figure 3d).

We note that the low concentration of $Ir(ppy)_3$ may lead to a Förster-type TTA with $k_{TT,g}$ of about 1×10^{-13} cm^{-3} s^{-1},[5] so the guest−guest TTA (with k_{TT} of 3×10^{-12} cm^{-3} s^{-1}) is not underestimated, even though the TTA quenching rates for $Ir(ppy)_3$ are much lower (<6.2%, Figure 4e) than the triplet radiative rates owing to the relatively low triplet density, leading to a similar efficiency roll-off of $Ir(ppy)_3$'s emission ($n_{T,g}$) compared to that of the singlets in the PBICT host (n_S; Figure 4d). These results indicate that the efficiency loss in an efficient PH emitter of TSP OLEDs is very small. Thus, TSP can serve as a promise mechanism to realize the limiting $J_{1/2}$ of 40 A cm^{-2}. $J_{1/2}$ extrapolated from the simulation curves (Figure 4b) also increase with increasing k_{FRET}. All of these results well support our theory of suppressing the efficiency roll-off by using TSP. A maximum $J_{1/2}$ of 460 mA cm^{-2} is obtained at 5 wt % $Ir(ppy)_3$. To the best of our knowledge, this $J_{1/2}$ is much larger than that of the reported TADF devices (Figure S1 in the SI). At EQE of 23.1%, $J_{90\%}$ is larger than those of the reported OLEDs (Figure S6 in the SI).

As can be inferred from Figure 3, decreasing ΔE_{ST} leads to increasing IQE and $J_{1/2}$. To further confirm this, we replaced PBICT with 2,4-diphenyl-6-bis(12-phenylindolo)[2,3-*a*]-carbazol-11-yl)-1,3,5-triazine (DIC-TRZ) as the host material in the same device structure. ΔE_{ST} of DIC-TRZ is 0.06 eV.[28] As depicted in Figure 4f, both EQE and $J_{1/2}$ of the DIC-TRZ/$Ir(ppy)_3$ device are improved.

In summary, we find that the efficiency roll-off of the TADF OLEDs is mainly caused by STA and TTA. It is always serious because small ΔE_{ST} is always followed by small k_S, so a low triplet density is hard to realize. We show that the strategy of TSP can simultaneously realize high efficiency and low efficiency roll-off by replacing the small k_S with the much larger k_{FRET}. The TSP device using the PBICT/$Ir(ppy)_3$ system realizes $J_{1/2}$ of 460 mA cm^{-2} at EQE of 23.1%, and the superior efficiency roll-off is well explained by the exciton dynamics model. Further works will be focused on developing host materials (including molecules and exciplexes) with smaller ΔE_{ST} and host−guest systems with larger spectral integrals.

■ ASSOCIATED CONTENT

Supporting Information

Methods, Figures S1−S6, and Tables S1 and S2. The Supporting Information is available free of charge on the ACS Publications website at DOI: 10.1021/acsami.5b04090.

■ AUTHOR INFORMATION

Corresponding Author

*E-mail: duanl@mail.tsinghua.edu.cn.

Notes

The authors declare no competing financial interest.

■ ACKNOWLEDGMENTS

The authors thank the National Natural Science Foundation of China (Grants 51173096 and 61177023) and the National Basic Research Program (Grant 2015CB655002) for financial support.

■ REFERENCES

(1) Reineke, S.; Thomschke, M.; Lüssem, B.; Leo, K. White Organic Light-Emitting Diodes: Status and Perspective. *Rev. Mod. Phys.* **2013**, *85*, 1245−1293.

(2) Riehemann, S.; Grossmann, C.; Vogel, U.; Richter, B.; Herold, R.; Notni, G. Ultra Small OLED Pico Projector. *Opt. Photonik* **2009**, *4*, 34−36.

(3) Baldo, M. A.; Holmes, R. J.; Forrest, S. R. Prospects for Electrically Pumped Organic Lasers. *Phys. Rev. B: Condens. Matter Mater. Phys.* **2002**, *66*, 035321-1−035321-16.

(4) Murawski, C.; Leo, K.; Gather, M. C. Efficiency Roll-Off in Organic Light-Emitting Diodes. *Adv. Mater.* **2013**, *25*, 6801−6827.

(5) Baldo, M. A.; Adachi, C.; Forrest, S. R. Transient analysis of Organic Electrophosphorescence. II. Transient Analysis of Triplet-Triplet Annihilation. *Phys. Rev. B: Condens. Matter Mater. Phys.* **2000**, *62*, 10967−10977.

(6) Adachi, C.; Baldo, M. A.; Thompson, M. E.; Forrest, S. R. Nearly 100% Internal Phosphorescence Efficiency in an Organic Light-Emitting Device. *J. Appl. Phys.* **2001**, *90*, 5048−5051.

(7) Forrest, S. R.; Baldo, M. A.; O'Brien, D. F.; You, Y.; Shoustikov, A.; Sibley, S.; Thompson, M. E. Highly Efficient Phosphorescent Emission from Organic Electroluminescent Devices. *Nature* **1998**, *395*, 151−154.

(8) Jeon, S.-O.; Yook, K. S.; Joo, C. W.; Lee, J. Y.; Ko, K.-Y.; Park, J.-Y.; Baek, Y. G. 100% Internal Quantum Efficiency and Stable Efficiency Roll-Off in Phosphorescent Light-Emitting Diodes Using a High Triplet Energy Hole Transport Material. *Appl. Phys. Lett.* **2008**, *93*, 063306-1−063306-3.

(9) Song, D.; Zhao, S.; Luo, Y.; Aziz, H. Causes of Efficiency Roll-Off in Phosphorescent Organic Light Emitting Devices: Triplet−Triplet Annihilation versus Triple−-Polaron Quenching. *Appl. Phys. Lett.* **2010**, *97*, 243304-1−243304-3.

DOI: 10.1021/acsami.5b04090
ACS Appl. Mater. Interfaces 2015, 7, 15154−15159

(10) Rothe, C.; King, S. M.; Monkman, A. P. Direct Measurement of the Singlet Generation Yield in Polymer Light-Emitting Diodes. *Phys. Rev. Lett.* **2006**, *97*, 076602-1−076602-4.
(11) Pope, M.; Magnante, P.; Kallmann, H. P. Electroluminescence in Organic Crystals. *J. Chem. Phys.* **1963**, *38*, 2042−2042.
(12) Zhang, Y.; Forrest, S. R. Triplets Contribute to Both an Increase and Loss in Fluorescent Yield in Organic Light Emitting Diodes. *Phys. Rev. Lett.* **2012**, *108*, 267404-1−267404-5.
(13) Wallikewitz, B. H.; Kabra, D.; Gelinas, S.; Friend, R. H. Triplet Dynamics in Fluorescent Polymer Light-Emitting Diodes. *Phys. Rev. B: Condens. Matter Mater. Phys.* **2012**, *85*, 045209-1−045209-15.
(14) Uoyama, H.; Goushi, K.; Shizu, K.; Nomura, H.; Adachi, C. Highly Efficient Organic Light-Emitting Diodes from Delayed Fluorescence. *Nature* **2012**, *492*, 234−238.
(15) Dias, F. B.; Bourdakos, K. N.; Jankus, V.; Moss, K. C.; Kamtekar, K. T.; Bhalla, V.; Santos, J.; Bryce, M. R.; Monkman, A. P. Triplet Harvesting with 100% Efficiency by Way of Thermally Activated Delayed Fluorescence in Charge Transfer OLED Emitters. *Adv. Mater.* **2013**, *25*, 3707−3714.
(16) Zhang, Q.; Li, B.; Huang, S.; Nomura, H.; Tanaka, H.; Adachi, C. Efficient Blue Organic Light-Emitting Diodes Employing Thermally Activated Delayed Fluorescence. *Nat. Photonics* **2014**, *8*, 326−332.
(17) Zhang, D.; Duan, L.; Zhang, D.; Qiu, Y. Towards Ideal Electrophosphorescent Devices with Low Dopant Concentrations: The Key Role of Triplet Up-Conversion. *J. Mater. Chem. C* **2014**, *2*, 8983−8989.
(18) Kasemann, D.; Brückner, R.; Fröb, H.; Leo, K. Organic Light-Emitting Diodes under High Currents Explored by Transient Electroluminescence on the Nanosecond Scale. *Phys. Rev. B: Condens. Matter Mater. Phys.* **2011**, *84*, 115208-1−115208-8.
(19) Wetzelaer, G. A. H.; Kuik, M.; Nicolai, H. T.; Blom, P. W. M. Trap-Assisted and Langevin-Type Recombination in Organic Light-Emitting Diodes. *Phys. Rev. B: Condens. Matter Mater. Phys.* **2011**, *83*, 165204-1−165204-5.
(20) Babenko, S. D.; Benderskii, V. A.; Gol'danskii, V. L.; Lavrushko, A. G.; Tychinskii, V. P. Annihilation of Singlet Excited States in Anthracene Solutions. *Chem. Phys. Lett.* **1971**, *8*, 598−600.
(21) Zhang, Y.; Whited, M.; Thompson, M. E.; Forrest, S. R. Singlet-Triplet Quenching in High Intensity Fluorescent Organic Light Emitting Diodes. *Chem. Phys. Lett.* **2010**, *495*, 161−165.
(22) Watanabe, S.; Furube, A.; Katoh, R. Generation and Decay Dynamics of Triplet Excitons in Alq_3 Thin Films under High-Density Excitation Conditions. *J. Phys. Chem. A* **2006**, *110*, 10173−10178.
(23) Reineke, S.; Walzer, K.; Leo, K. Triplet-Exciton Quenching in Organic Phosphorescent Light-Emitting Diodes with Ir-Based Emitters. *Phys. Rev. B: Condens. Matter Mater. Phys.* **2007**, *75*, 125328-1−125328-13.
(24) Masui, K.; Nakanotani, H.; Adachi, C. Analysis of Exciton Annihilation in High Efficiency Sky-Blue Organic Light-Emitting Diodes with Thermally Activated Delayed Fluorescence. *Org. Electron.* **2013**, *14*, 2721−2726.
(25) Goushi, K.; Yoshida, K.; Sato, K.; Adachi, C. Organic Light-Emitting Diodes Employing Efficient Reverse Intersystem Crossing For Triplet-To-Singlet State Conversion. *Nat. Photonics* **2012**, *6*, 253−258.
(26) Prezhdo, O. V.; Rossky, P. J. Evaluation of Quantum Transition Rates from Quantum-Classical Molecular Dynamics Simulations. *J. Chem. Phys.* **1997**, *107*, 5863−5878.
(27) Nakanotani, H.; Higuchi, T.; Furukawa, T.; Masui, K.; Morimoto, K.; Numata, M.; Tanaka, H.; Sagara, Y.; Yasuda, T.; Adachi, C. High-Efficiency Organic Light-Emitting Diodes with Fluorescent Emitters. *Nat. Commun.* **2014**, *5*, 4016.
(28) Zhang, D.; Duan, L.; Li, C.; Li, Y.; Li, H.; Zhang, D.; Qiu, Y. High-Efficiency Fluorescent Organic Light-Emitting Devices Using Sensitizing Hosts with a Small Singlet-Triplet Exchange Energy. *Adv. Mater.* **2014**, *26*, 5050−5055.
(29) Latt, S. A.; Cheung, H. T.; Blout, E. R. Energy Transfer - A System with Relatively Fixed Donor-Acceptor Separation. *J. Am. Chem. Soc.* **1965**, *87*, 995−1003.
(30) Sajoto, T.; Djurovich, P. I.; Tamayo, A. B.; Oxgaard, J.; Goddard, W. A., III; Thompson, M. E. Temperature Dependence of Blue Phosphorescent Cyclometalated Ir(III) Complexes. *J. Am. Chem. Soc.* **2009**, *131*, 9813−9822.

DOI: 10.1021/acsami.5b04090
ACS Appl. Mater. Interfaces 2015, 7, 15154−15159